地震研究所彙報
Bull. Earthq. Res. Inst.
Univ. Tokyo
Vol. 78 (2003) pp. 151–166

Repeating Slip Events at a Circular Asperity: Numerical Simulation with a Rate- and State-Dependent Friction Law

Naoyuki Kato*

Earthquake Research Institute, University of Tokyo

Abstract

I perform numerical simulation of slip process on a two-dimensional planar fault in an infinite uniform elastic medium using a rate- and state-dependent friction law. A circular patch with velocity-weakening frictional property is embedded in the fault, while velocity-strengthening frictional property is assumed in the other region. Simulation results indicate that slip events repeatedly occur at the velocity-weakening patch and slower slip propagates outwards in the velocity-strengthening region. The characteristics of simulated slip on the fault patch are controlled by the ratio of the patch radius r to the critical fault radius r_c, which is the critical nucleation patch radius for unstable slip, and is defined as a function of frictional constitutive parameters. When $r \gg r_c$, ordinary earthquakes with high slip rates repeatedly occur at the fault patch and postseismic aseismic slip follows on the fault outside the patch. When $r \sim r_c$, episodic aseismic slip events (silent earthquakes) occur. The rise time of the episodic event increases with a decrease in r/r_c. When $r \ll r_c$, stable sliding occurs. These results indicate that the r_c value can be estimated from geodetically determined values of the fault radius and the source duration of an episodic aseismic slip event.

Key words: episodic aseismic slip event, repeating earthquake, postseismic sliding, friction

1. Introduction

Earthquake source processes revealed from seismic waveform analyses of large earthquakes indicate that the slip amount on a fault is significantly nonuniform (e.g., Lay and Kanamori, 1981; Thatcher, 1990). The region of a relatively large seismic slip during an earthquake has often been called an asperity, which was originally used in rock mechanics to express a strong contact area on sliding surfaces (Byerlee, 1970). Recent geodetic observations indicate that significant aseismic sliding often follows a large earthquake (e.g., Kawasaki *et al.*,1995; Heki *et al.*, 1997). The postseismic sliding seems to occur mainly in the neighboring regions of asperities (Yagi *et al.*, 2001). Moreover, episodic aseismic slip events on plate interfaces have been detected with GPS observations (e.g., Hirose *et al.*, 1999; Dragert *et al.*, 2001).

These observations suggest that the frictional property on a plate interface is nonuniform. Stick-slip behavior occurs at some patches, which correspond to asperities, and aseismic sliding occurs in the other regions. Furthermore, the rupture propagation speeds in stick-slip events in the Earth show a wide variety. The most easily detected obvious slip events are ordinary earthquakes, whose rupture propagates at almost shear-wave speed. Ordinary earthquakes radiate significant high-frequency seismic waves. Slip events with slower rupture propagation speeds may be divided into slow and silent earthquakes (e.g., Beroza and Jordan, 1990). Slow earthquakes generate much larger amplitude long-period seismic waves than those expected from the amplitudes of short-period waves, and silent earthquakes generate no

*e-mail: nkato@eri.u-tokyo.ac.jp, (1–1–1 Yayoi, Bunkyo-ku, Tokyo 113–0032, Japan)

detectable short-period seismic waves and can be found with very long period seismometers, strainmeters, or GPS observations. The durations of rupture of slow and silent earthquakes are thought to be much longer than l/β, where l represents the fault dimension and β is the S-wave speed. Postseismic sliding and episodic aseismic slip events recently detected with GPS may be categorized into silent earthquakes.

Laboratory-derived rate- and state-dependent friction laws developed by Dieterich (1979) and Ruina (1983) are useful for understanding seismic and aseismic slip on a fault. The condition for the occurrence of seismic slip has been discussed theoretically in terms of the constitutive parameters of friction laws (Ruina, 1983; Rice and Ruina, 1983). The rate- and state-dependent friction laws have been successively applied to understand laboratory observations of rock friction, and to interpret field data of fault slip as reviewed by Marone (1998). From numerical simulations with a model of two-degree-of-freedom spring-block system obeying a rate- and state-dependent friction law, Yoshida and Kato (2003) examined the conditions for the occurrence of postseismic slip and episodic aseismic slip events. Furthermore, friction laws have been applied to modeling seismic cycles on a plate interface (Tse and Rice, 1986; Stuart, 1988; Rice, 1993; Stuart and Tullis, 1995; Kato and Hirasawa, 1997, 1999; Kuroki *et al.*, 2002). Among them, Kato and Hirasawa (1997) showed that ordinary, slow, and silent earthquakes can be simulated with the rate- and state-dependent friction law and Kato and Hirasawa (1999) examined the effect of spatial nonuniformity in frictional constitutive parameters on interplate sliding behavior with a 2D subduction zone model.

In the present paper, I perform numerical simulations of slip on a fault with the rate- and state-dependent friction law. Nonuniformity of frictional properties is introduced to simulate seismic slip at an asperity and aseismic slip outside the asperity. Through the numerical simulation, I examine the conditions for the occurrence of seismic slip events and episodic aseismic slip events and interactions between an asperity and the other regions.

2. The Model

I consider a two-dimensional (2D) planar square fault in an infinite uniform elastic medium with rigidity G and Poisson's ratio ν. Cartesian coordinates (x, y) are taken on the fault plane $z=0$ as shown in Fig. 1. I assume that the fault is loaded at a constant rate so that slip occurs at a slip rate V_{pl} in the x-direction. In the present paper, only shear stress τ_{zx} and slip u in the x-direction are considered, and τ_{zx} is expressed by τ for simplicity. The shear stress on the fault at a point (x, y) at a time t due to quasi-static slip u can be expressed by

$$\tau(x,y)=\int\int f(x-\xi,y-\eta)\,[u(\xi,\eta)-V_{pl}t]\,d\xi d\eta, \quad (1)$$

where $f(x-\xi, y-\eta)$ is shear stress at (x, y) due to unit slip at (ξ, η) in the x-direction. During seismic slip, quasi-static solution (1) cannot be applied because of the inertia effect. In the present paper, the inertia effect is approximately evaluated by introducing a radiation damping approximation (Rice, 1993) for the purpose of efficient numerical computation. The shear stress is written by

$$\tau(x,y)=\int\int f(x-\xi,y-\eta)\,[u(\xi,\eta)-V_{pl}t]\,d\xi d\eta-\frac{G}{2\beta}V(x,y), \quad (2)$$

where $V=du/dt$ is the slip rate on the fault and β is the S-wave speed. When the fault plane is discretised with many equal-area square cells each with uniform slip, the shear stress at the center of cell (i, j) is written from (2) by

$$\tau(i,j)=\sum_{k,l}K(i-k,j-l)\,[u(k,l)-V_{pl}t]-\frac{G}{2\beta}V(i,j), \quad (3)$$

where $K(i-k, j-l)$ is given in Appendix A. In the numerical simulation, the summation in (3) is efficiently evaluated using the 2D FFT technique.

The frictional stress acting on the fault is assumed to obey the composite rate- and state-dependent friction law (Kato and Tullis, 2001; 2003):

$$\tau=\mu\sigma_n^{eff}, \quad (4\,a)$$

$$\mu=\mu_*+a\ln(V/V_*)+b\ln(V_*\theta/D_c), \quad (4\,b)$$

$$\frac{d\theta}{dt}=\exp\left(-\frac{V}{V_0}\right)-\left(\frac{V\theta}{D_c}\right)\ln\left(\frac{V\theta}{D_c}\right), \quad (4\,c)$$

where μ is a friction coefficient, σ_n^{eff} is effective normal stress, θ is a state variable representing a contact state of fault surfaces or an internal structure of a gouge zone between fault surfaces, a, b, D_c and V_0 are constants, which characterize frictional properties, and V_* and μ_* are arbitrarily chosen reference veloc-

ity and frictional coefficient, which do not affect simulated slip behavior in the present model. Following Kato and Tullis (2001, 2003), I take V_0 to be 10^{-8} m/s in all cases using experimental data for granite surfaces of Blanpied *et al.* (1998).

Using a rate- and state-dependent friction law and a single-degree-of-freedom spring block system, Rice and Ruina (1983) and Ruina (1983) theoretically analyzed the stability of the system. They found that unstable (seismic) slip may occur when the steady-state friction shows velocity weakening ($a-b<0$) and the spring stiffness is smaller than a critical value k_c:

$$k_c=(b-a)\sigma_n^{eff}/D_c. \tag{5}$$

When $a-b$ is positive (velocity strengthening) or the spring stiffness is larger than k_c, stable sliding occurs. Episodic sliding is expected to occur when the stiffness is nearly equal to k_c. For a finite fault in an elastic medium, an effective stiffness k^{eff} of a fault may be defined by

$$k^{eff}=\Delta\tau/\Delta u, \tag{6}$$

where $\Delta\tau$ is the stress change due to slip Δu on the fault (e.g., Dieterich, 1992). For a square fault with uniform slip in an infinite uniform Poissionian ($\nu=0.25$) elastic medium, k^{eff} is given by

$$k^{eff}=\frac{7\sqrt{2}}{3\pi}\frac{G}{l}, \tag{7}$$

where l is the length of the fault (See Eq. (A 6) in Appendix A). From (5) and (7), the critical fault length l_c can be defined by

$$l_c=\frac{7\sqrt{2}}{3\pi}\frac{G}{(b-a)\sigma_n^{eff}}D_c. \tag{8}$$

In the present paper, the variation of σ_n^{eff} with time is not taken into consideration. I introduce new parameters $A\equiv a\sigma_n^{eff}$ and $B\equiv b\sigma_n^{eff}$ for simplicity. Then l_c is expressed by

$$l_c=\frac{7\sqrt{2}}{3\pi}\frac{G}{(B-A)}D_c. \tag{9}$$

Similarly, for a circular shear crack with a constant stress drop, k^{eff} is given from Eshelby's (1957) elastic solution by

$$k^{eff}=\frac{7\pi}{24}\frac{G}{r}, \tag{10}$$

where r is a fault radius. The critical fault radius r_c can be defined by

$$r_c=\frac{7\pi}{24}\frac{G}{(B-A)}D_c. \tag{11}$$

A fault whose length or radius is larger than l_c or r_c

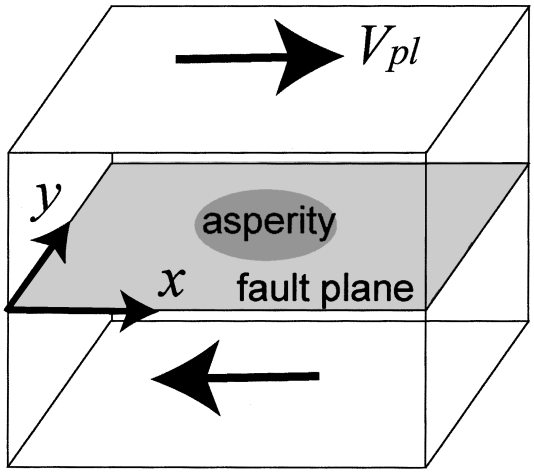

Fig. 1. An illustration of a two-dimensional planar fault on the xy-plane in an infinite uniform elastic medium. The fault is loaded by a constant plate velocity V_{pl} in the x-direction.

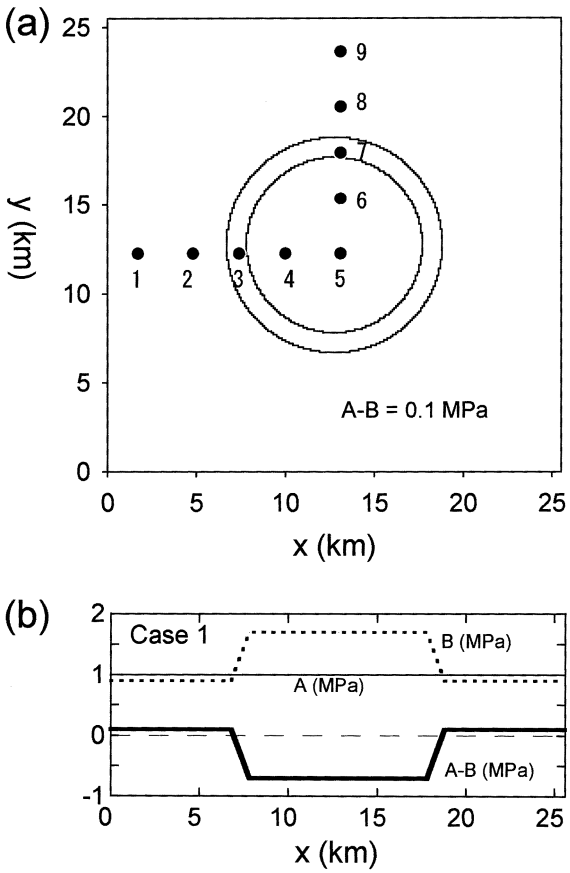

Fig. 2. (a) Map view of the model fault. The value of $A-B$ in the inner circle is a negative constant and that in the outside of the outer circle is 0.1 MPa. The $A-B$ value in the region between the inner and the outer circle linearly changes with the distance from the center of the circles. Numerals 1 to 9 are points where simulated slip or stress histories are shown in Fig. 3 to 16. (b) The variation of A, B, and $A-B$ with x for $y=12.8$ km for Case 1.

corresponds to a weak stiffness elastic system with $k<k_c$, therefore, unstable slip is expected to occur on the fault. On the other hand, stable sliding is expected to occur on a fault that is smaller than l_c or r_c.

In the simulation, the characteristic slip distance D_c is assumed to be 0.05 m uniform over the model fault in an infinite uniform elastic medium with $G=30$ GPa, $\nu=0.25$, and $\beta=3$ km/s. Although the assumed D_c value of 0.05 m is much larger than laboratory values (e.g., Dieterich, 1979), it is comparable to assumed values for natural faults in preceding simulation studies (e.g., Tse and Rice, 1986; Stuart, 1988; Kato and Hirasawa, 1997). Since D_c depends on the characteristic scale of roughness of sliding surfaces or the gouge layer between sliding surfaces in the laboratory, it is believed to have larger values in natural faults than in the laboratory (e.g., Marone and Kilgore, 1993). Nondimensional quantities such as distances $X=x/D_c$ and $Y=y/D_c$, displacement $U=u/D_c$, and time $T=V_*t/D_c$ are used in numerical computations. The simulation results shown below may be applied for larger or smaller scale faults by changing the value of D_c and multiplying the factor for D_c to distance, displacement, and time scales. The plate velocity V_{pl} is assumed to be 0.1 m/yr, and the reference velocity V_* is taken to be the same as the plate velocity V_{pl} (=0.1 m/yr). The square fault is divided into 65536 (256×256) cells, whose sizes are $\Delta x=\Delta y=100$ m ($\Delta X=\Delta Y=2000$). The periodic boundary condition is assumed.

The spatial distribution of $A-B$ assumed in the simulation is schematically shown in Fig. 2 a. $A-B$ is a constant negative value in a circular patch with a radius of 5 km ($=50\Delta 2X=10^5 D_c$) and the center of $(x, y)=(12.8\text{ km}, 12.8\text{ km})$. The value of $A-B$ is a constant positive value (0.1 MPa) for the distance from the center of a patch larger than 6 km. The value of $A-B$ linearly changes with the distance from the center for 5 km to 6 km. Seven numerical simulations are examined in the present paper (Table 1). The distributions of A, B, and $A-B$ for Case 1 are displayed in Fig. 2 b. In all cases $A=1.0$ MPa is uniform over the fault and B is nonuniform. $B=0.9$ MPa for the distance from the center of a circular patch larger than 6 km in all cases. Since laboratory values of a and b are around 0.01 for granite surfaces at room temperatures (e.g., Blanpied *et al.*, 1998), the assumed A and B values correspond to σ_n^{eff} of about 100 MPa. The cell size Δx must be much smaller than l_c as shown by Rice (1993) to avoid numerical instability. l_c for $A-B=-0.7$ MPa and $D_c=0.05$ m is 2251 m, which is the minimum value in all models. In this study Δx is always smaller than $0.05\,l_c$, which satisfies the numerical stability condition. The critical fault radius r_c is calculated for each case as shown in Table 1 for friction parameters in the circular patch with a negative $A-B$ value.

The patch radius r relative to r_c is expected to control sliding behavior as indicated by the above theory. Kato and Hirasawa (1997) have shown for a 2

Table 1. Model parameters for seven numerical simulations and the recurrence interval T_r of simulated earthquakes.

Case	*A-B* (MPa)	r_c (km)	r/r_c	T_r (years)
1	-0.7	1.96	2.55	28.3
2	-0.5	2.75	1.82	28.5, 17.2
3	-0.3	4.58	1.09	16.2
4	-0.14	9.82	0.51	14.5
5	-0.12	11.45	0.44	12.9 12.7
6	-0.08	17.18	0.29	12.0
7	-0.05	27.89	0.18	-

A-B; the value in the circular patch.

r_c; the value calculated with Eq. (11) and the value of *A-B* in the circular patch.

r/r_c; r (= 5 km) is the radius of the circular patch with a constant negative *A-B* value.

T_r; the recurrence interval of slip events in a circular patch with a negative *A-B* value.

D subduction zone numerical model that the length l of seismogenic zone with velocity-weakening frictional property to the critical fault length l_c controls the seismic coupling coefficient χ, which is the ratio of seismic slip to total slip during a seismic cycle. They found that earthquakes repeatedly occur and χ is close to 1 for $l/l_c \gg 1$, and stable sliding occurs and $\chi=0$ for $l/l_c \ll 1$. Slow or silent earthquakes occur when l/l_c is close to 1. In the present paper, sliding behavior is examined in more detail with a 3D model by changing r_c relative to the patch radius r with a constant negative $A-B$ value (Table 1).

The initial condition is that $\tau=\tau_*+(A-B)\ln(V/V_*)$ with the initial sliding velocity $V_{init}=0.1\,V_{pl}$, where $\tau_*=\mu_*\sigma_n^{eff}$. Numerical simulations are done by solving friction equations (4 a) to (4 c) with the Runge-Kutta method (Press *et al.*, 1992) coupled with Eq. (3). Simulated slip histories show steady periodic behavior after some unsteady behavior due to the artificial initial condition. The simulation results in the next section are those for about 100 years from the initial state.

3. Numerical Simulation Results

Simulated slip histories for seven cases (Table 1) are shown for nine points on the fault (Fig. 2 a). Points 4, 5, and 6 are in the circular patch with a negative $A-B$ value; 1, 2, 8, and 9 are in the positive $A-B$ region; and, 3 and 7 are in the region of transitional value of $A-B$. Note that slip occurs in the x-direction, therefore, slip propagates in an in-plane shear mode along Points 1 to 5 and in an anti-plane shear mode along Points 5 to 9.

Simulated slip histories for Case 1 ($r/r_c=2.55$) are shown in Fig. 3, where four events are included. Simulated slip behavior is periodic. Characteristics of silent event 1 and earthquake 1 are the same as those of silent event 2 and earthquake 2, respectively. The same characteristic events repeatedly occur at a constant time interval $T_r=28.3$ years. Slip histories during an earthquake are shown in Fig. 4 on an expanded time scale. Slip amounts at Points 4, 5, and 6 in the circular patch are nearly the same, and the slip amplitude decreases with the distance from the center of the patch. In the positive $A-B$ region, significant postseismic slip occurs. Fig. 5 shows seismic slip on a further expanded time scale, indicating that the slip rise time in the negative $A-B$ region is several seconds. Seismic slip occurs because the patch size of a velocity-weakening region is much longer than the critical size r_c. Slip behavior during

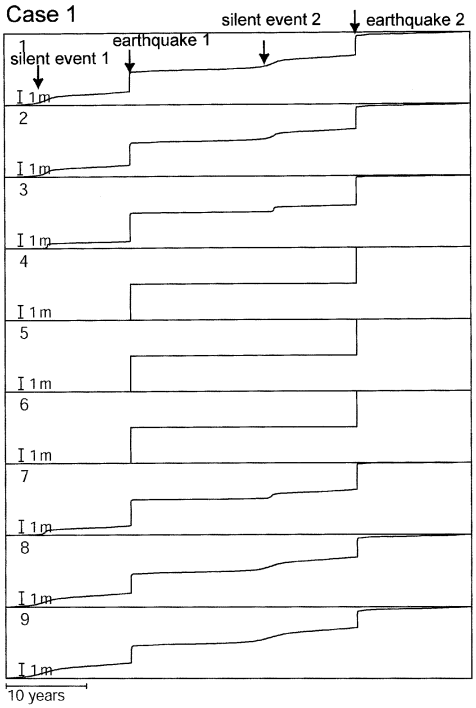

Fig. 3. Simulated slip histories at nine points on the fault for Case 1.

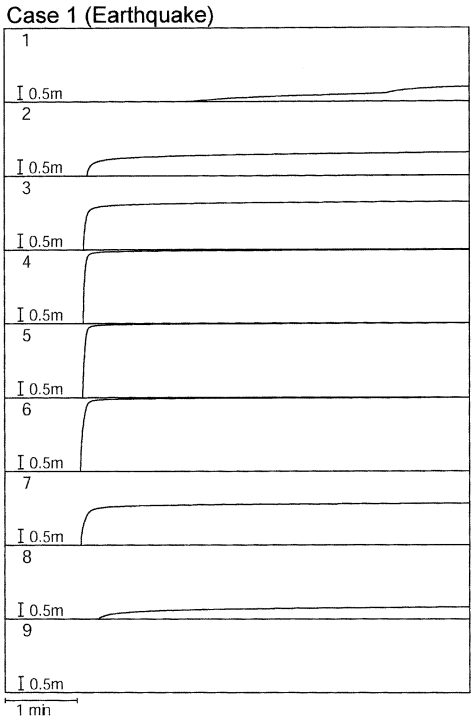

Fig. 4. Simulated slip histories during the occurrence of an earthquake for Case 1 on an expanded time scale.

a silent event is displayed in Fig. 6. The circular patch with negative $A-B$ value is locked during the event, while nearly steady sliding occurs in the positive $A-B$ region. Significant episodic slip takes place at points 3 and 7, where $A-B$ takes transitional values, and it cannot propagate into the stronger circular patch with a more negative $A-B$ value than those in the transitional zone. The effective stiffness of the annular transitional zone is evaluated to be 35 MPa/m in Appendix B, while the critical stiffness k_c for $A-B=-0.7$ MPa and $D_c=0.05$ m is 14 MPa/m from Eq. (5). The effective stiffness k_{eff} of the annular region is on the same order of magnitude as k_c, suggesting that slip at the annular region may be an episodic aseismic event. The episodic slip at the annular region with transitional $A-B$ values is discussed again in the next section.

Figure 7 shows simulated slip histories for Case 2 ($r/r_c=1.82$), where two ordinary earthquakes and a silent event occur during the time interval. Slip behavior shown in Fig. 7 repeatedly occurs in the simulation. The magnitude of earthquake 2 is larger than that of earthquake 1, therefore, three types of event are included during a cycle in this case. The earthquake recurrence intervals T_r are 28.5 years (earthquake 1 to 2) and 17.2 years (earthquake 2 to 1). The phenomenon whereby the different types of slip events alternate with each other is known as period doubling bifurcation (e.g., Gu *et al.,* 1984), which is discussed in the next section. Both in earthquakes 1 and 2, seismic slip occurs at Points 4 to 6 in the circular region with frictional property of velocity weakening and significant postseismic sliding propagates outwards in the velocity-strengthening friction region. During silent event 1, the most rapid episodic slip occurs at points 3 and 7 in the region of transitional property of friction. These characteristics are similar to those of earthquakes and silent events in Case 1.

Simulated slip histories for Case 3 ($r/r_c=1.09$) are shown in Fig. 8. In this case, no significant episodic slip event occurs during an interseismic period. Figs. 9 and 10 show slip histories on expanded time scales. The rise time of postseismic slip at Point 2 in the velocity-strengthening friction region for Case 1 (Fig. 4) is a few minutes, while that for Case 3 (Fig. 9) is about 1 day. This indicates that the characteristics of postseismic slip for the two cases are significantly different from each other. However, Figs. 5 and 10 show that the duration of seismic slip in Case 3 is nearly the same as that in Case 1.

I observe periodic occurrence of earthquakes in the circular patch with outgoing postseismic sliding in Case 4 ($r/r_c=0.51$). No episodic slip event is found during an interseismic period in this case as well as in Case 3. Fig. 11 shows slip histories during seismic slip for Case 4, indicating that the slip rise time is significantly longer than those of Cases 1 and 3 (Figs. 5 and 10). Extraordinarily long slip duration for a patch radius of 5 km in this case indicates that the event is a slow earthquake. This is discussed quantitatively in the next section.

Figure 12 shows simulated slip histories for Case 5 ($r/r_c=0.44$), demonstrating that two types of silent event alternately occur. Characteristics of silent events 1 and 2 are almost the same as those of silent events 3 and 4, respectively. The time intervals T_r between silent events are 12.9 years (silent events 1 to 2 or 3 to 4) and 12.7 years (silent events 2 to 3). Figs. 13 and 14 show slip histories of silent events 1 and 2, respectively. The duration of silent event 1 is much shorter than that of silent event 2. Fig. 14 indicates that significant slip occurs twice in the velocity-weakening circular region (Points 4 to 6) during silent even 2. When the first slip event reaches the boundary of the model fault, the boundary reflects slip, generating the second slip event. Thus, the second slip event during silent event 2 is probably an artificial event due to the insufficient distance from the circular patch to the boundary of the model fault.

Simulated slip histories for Case 6 ($r/r_c=0.29$) is shown in Fig. 15, which includes two silent events. Characteristics of events 1 and 2 are almost the same. The duration of the event is longer than those of silent events in Case 5. In this case, nearly the same types of event repeatedly occur. However, the magnitude of event and the recurrence interval gradually decreases with time. Because the decrease rates of magnitude and recurrence interval are smaller than 1% a cycle, repeated slip events are observed during the time interval of the present simulation. The slip behavior may become stable for a longer time as will be seen for Case 7.

Figure 16 shows simulated histories of shear stress for Case 7 ($r/r_c=0.18$) from the beginning of the simulation. Episodic events occur at first and their

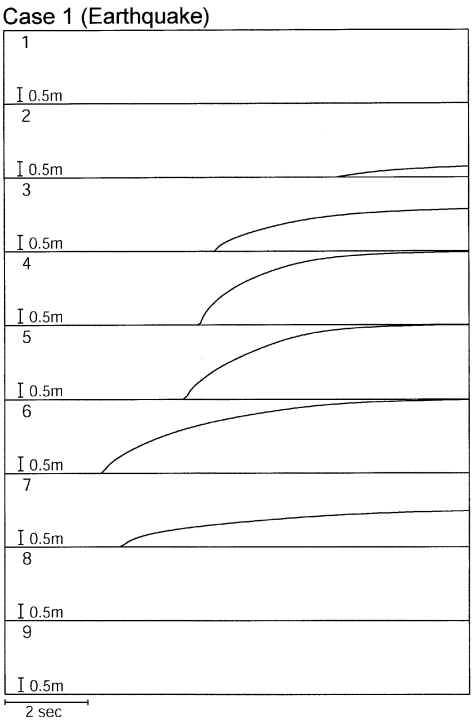

Fig. 5. Simulated slip histories during the occurrence of an earthquake for Case 1 on a further expanded time scale.

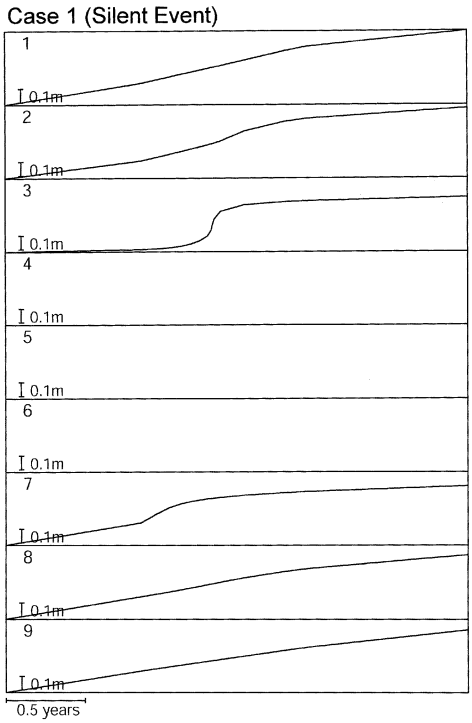

Fig. 6. Simulated slip histories during the occurrence of a silent event for Case 1 on an expanded time scale.

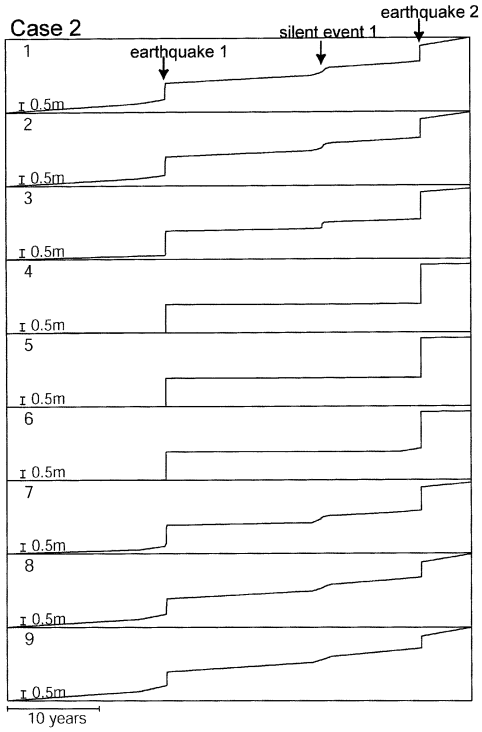

Fig. 7. Simulated slip histories for Case 2.

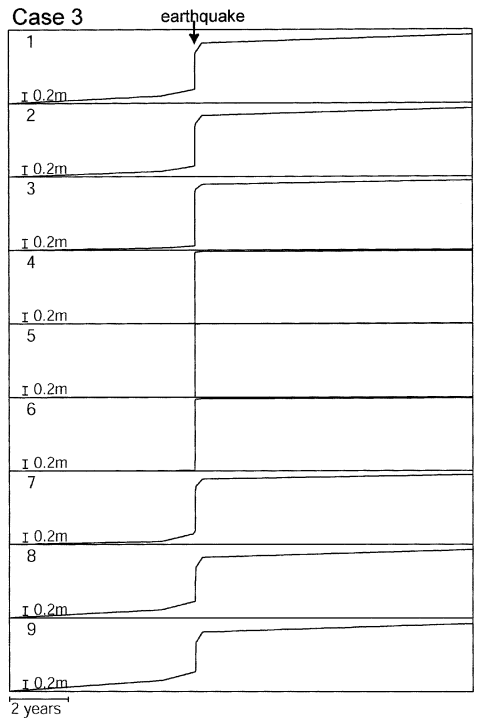

Fig. 8. Simulated slip histories for Case 3.

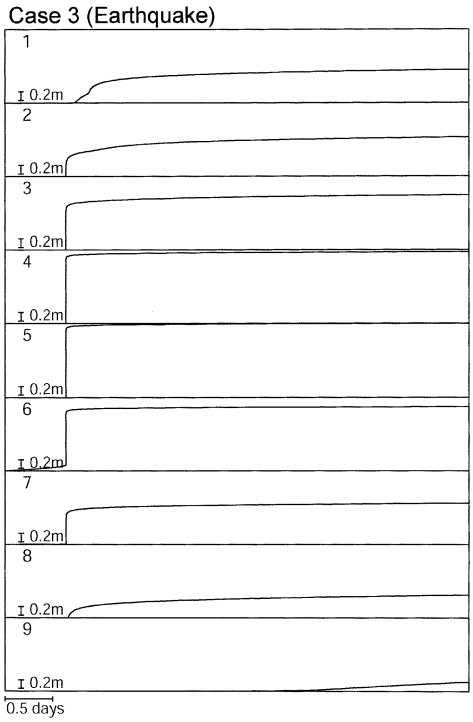

Fig. 9. Simulated slip histories during the occurrence of an earthquake for Case 3 on an expanded time scale.

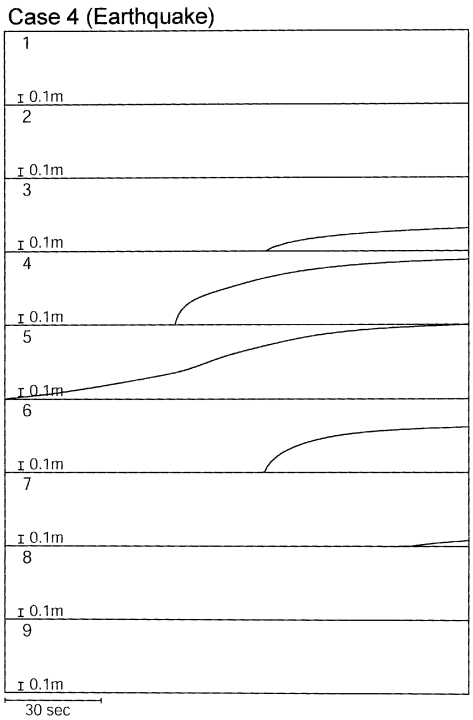

Fig. 11. Simulated slip histories during the occurrence of an earthquake for Case 4.

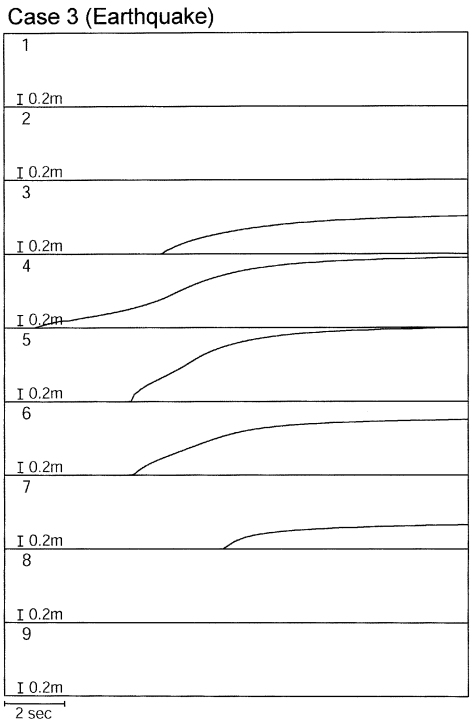

Fig. 10. Simulated slip histories during the occurrence of an earthquake for Case 3 on a further expanded time scale.

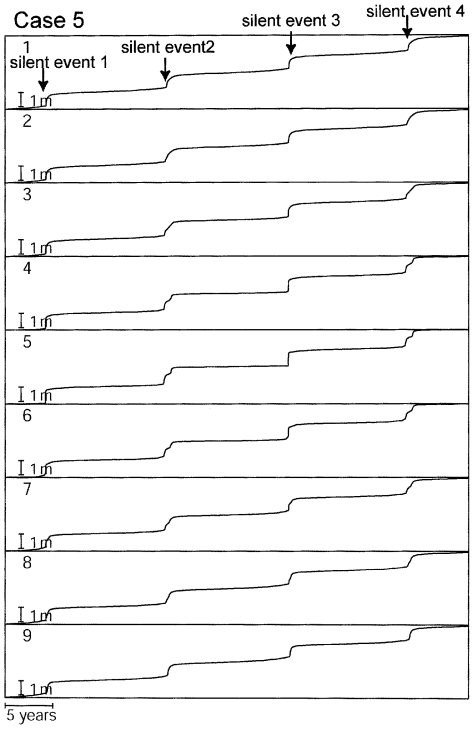

Fig. 12. Simulated slip histories for Case 5.

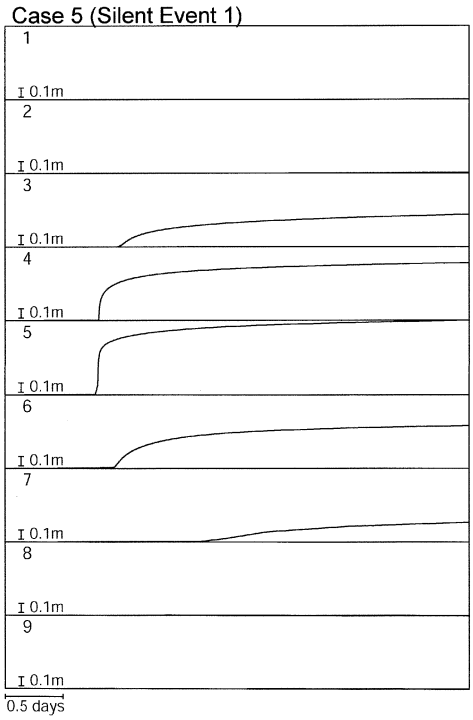

Fig. 13. Simulated slip histories during the occurrence of silent event 1 for Case 5 on an expanded time scale.

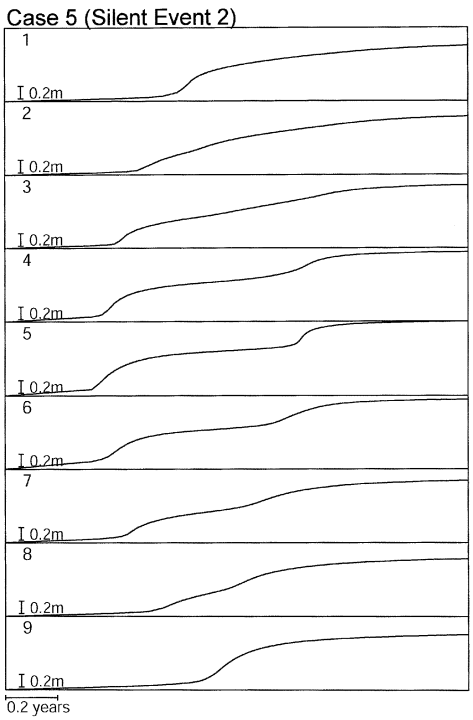

Fig. 14. Simulated slip histories during the occurrence of silent event 2 for Case 5 on an expanded time scale.

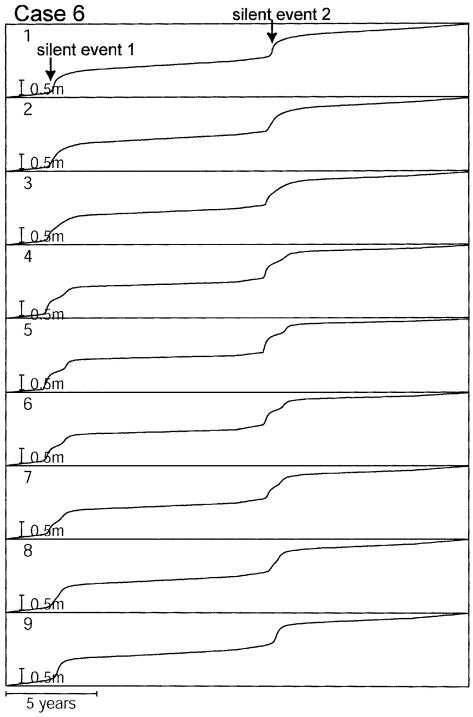

Fig. 15. Simulated slip histories for Case 6.

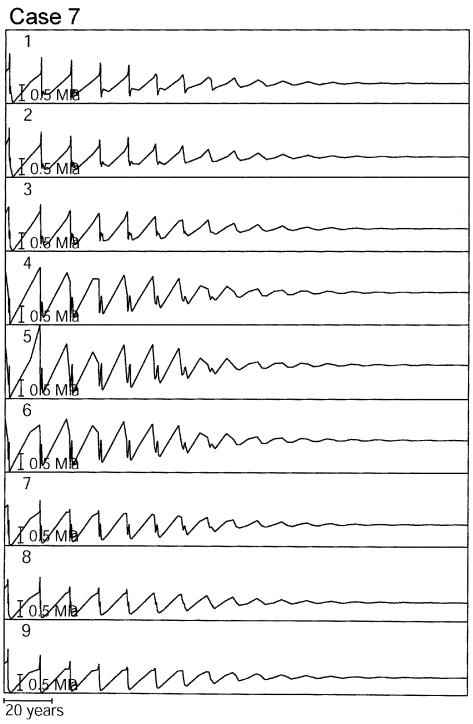

Fig. 16. Simulated shear-stress histories for Case 7.

amplitudes rapidly decrease with time. Finally, sliding becomes stable. This behavior is similar to that of a single-degree-of-freedom spring block model with a stiffness larger than k_c (Ruina, 1983).

The simulation results indicate that episodic slip is generated in and around the circular patch with a negative $A-B$ value and that slip behavior changes from rapid unstable slip (ordinary earthquakes), slow episodic slip (slow and silent earthquakes) to stable sliding with a decrease in r/r_c. This is consistent with the theoretical prediction discussed in the preceding section and numerical studies for a single-degree-of-freedom spring-block system (e.g., Gu *et al.*, 1984) and a 2D subduction zone model (Kato and Hirasawa, 1997).

4. Variation of Simulated Slip Events with Relative Patch Size

In this section, I discuss how simulated slip behavior varies with r/r_c, the ratio of the circular patch radius with a negative $A-B$ value to the critical patch radius, to understand the mechanism of ordinary, slow, and silent earthquakes. The recurrence interval T_r of slip events at the circular patch with a negative $A-B$ value is plotted against r/r_c in Fig. 17. Here, silent events at the perimeter of the circular patch are excluded from the discussion of recurrence interval for simplicity. T_r increases with r/r_c because a larger seismic slip occurs for a larger value of r/r_c. Since slip events with characteristics that differ from each other alternatively take place for $r/r_c \sim 0.4$ and 2, two T_r values exist (e.g., Cases 2 and 5).

Period doubling was found in numerical simulations for a single-degree-of-freedom spring-block system with a rate- and state-dependent friction law with two state variables (Gu *et al.*, 1984; Gu and Wong, 1994) and in laboratory experiments (e.g., Gu and Wong, 1994). In the friction law with two state variables θ_1 and θ_2, the magnitudes of variations of θ_1 and θ_2 are scaled with b_1 and b_2, respectively, and their evolutions with slip distance are scaled with D_{c1} and D_{c2}. Gu *et al.* (1984) reported that period doubling is found in their numerical simulation for $k/k_c \sim 0.86$, and unstable slip and permanently sustained oscillation are observed for smaller and larger stiffness, respectively. For $k/k_c > 1$, stable sliding is observed. Period doubling at $r/r_c \sim 0.4$ in the present simulation seems to correspond to that observed by Gu *et al.* (1984). When period doubling occurs at $r/r_c \sim 2$, episodic aseismic slip events are found in the region of transitional frictional property. The effective stiffness k_{eff} of the annular transitional region is estimated to be 35 MPa/m from an approximate elastic solution for slip on an annular crack (Appendix B). The critical stiffness k_c is 10 MPa/m for $A-B=-0.5$ MPa and $D_c=0.05$ m (Case 2). The value of k_c/k_{eff}, which corresponds to r/r_c, of the annular transitional zone for Case 2 is 0.29, which may generate period doubling as seen in Fig. 17. Thus, the period doubling at $r/r_c \sim 2$ seems to be related to the change in sliding behavior from stable to unstable at the transitional region.

In the present model, I use one state variable friction law, for which period doubling was not found in a single-degree-of-freedom spring-block system (Gu *et al.*, 1984) or in a 2D subduction zone model (Kato and Hirasawa, 1997). Mitsui and Hirahara (2001) found period doubling in their simulation of the motion of a single-degree-of-freedom spring-dashpot-block system with a rate- and state-dependent friction law, where they introduced a dashpot element to represent the viscoelasticity of material. They found period doubling, although they adopted a one state variable friction law. Nonlinear coupling between the load point and the block due to the dashpot element is a possible cause of period doubling in their model. Although the detailed mechanism of the occurrence of period doubling in the present model cannot be elucidated, it seems to be related to nonlinear interactions between slip in the region of velocity-weakening frictional property and that in the region of velocity-strengthening frictional property.

The duration of a simulated slip event is measured to judge whether the event is an ordinary, slow, or silent earthquake. Here, the duration is defined by the time interval from a rapid slip onset to 80% of final slip in the circular patch with a negative $A-B$ value, and it is read on simulated slip histories by the eye. It is difficult to strictly define the final slip; accordingly, the determined slip durations have some errors. However, these roughly estimated values are useful because they vary over many orders of magnitudes. Fig. 18 shows the slip duration versus r/r_c, indicating that it is nearly constant for $r/r_c > 1$ and it is rapidly increases with a decrease in r/r_c for

$r/r_c < \sim 1$. The slip durations for $r/r_c > 1$ are roughly consistent with the expected slip duration of a few seconds for an ordinary earthquake with a fault radius of 5 km (Beroza and Jordan, 1990), indicating that these simulated slip events are ordinary earthquakes. For r/r_c from about 0.5 to about 1, the slip durations are tens to hundreds of seconds, being significantly longer than the expected value for ordinary earthquakes. These correspond to slow earthquakes. The simulated slip events for $r/r_c < \sim 0.5$ have durations longer than 1 day, suggesting that these are silent earthquakes.

The transition from unstable slip to stable sliding in the present simulation occurs for r/r_c that is significantly smaller than 1.0. Dieterich (1992) performed a numerical simulation of slip nucleation process for a straight fault in a plane-strain elastic model with the slip law, whose frictional property at the nucleation phase is similar to the composite law used in the present study (Kato and Tullis, 2003), to find that the critical nucleation zone size observed in the simulation is smaller than the theoretical value given by (11). This is consistent with the above result for a smaller r/r_c-value at the sliding mode transition.

To measure the magnitudes of simulated slip events, I calculate seismic moment defined by

$$M_0 = G\int_S u_{V \geq Vc} dS, \qquad (12)$$

where $u_{V \geq Vc}$ is slip amount with slip rate equal to or greater than V_c, and S is the entire fault plane. Since the inertia is not rigorously evaluated in the present simulation, the seismic moment for high slip rates has a certain error. However, M_0 for various V_c values is useful for comparing the simulated slip events. The calculated M_0 values for $V_c = 1$ m/s, 0.01 m/s, and 10^{-4} m/s are plotted against r/r_c in Fig. 19. M_0 values for $V_c = 0.01$ m/s and 10^{-4} m/s gradually decrease with a decrease in r/r_c for $r/r_c > \sim 0.5$ and decrease more rapidly for $r/r_c < \sim 0.5$. The ratios of M_0 for $V_c = 1$ m/s to M_0 for $V_c = 0.01$ m/s and 10^{-4} m/s decrease with a decrease in r/r_c. For $r/r_c < \sim 1$, the ratios are smaller than 0.01. This indicates that the simulated slip events for $r/r_c < \sim 1$ are slow earthquakes. M_0 for $V_c = 1$ m/s and 0.01 m/s are zero for $r/r_c < \sim 0.5$, indicating that the events are silent earthquakes. These results are consistent with the classification of simulated slip events with slip duration.

5. Discussion and Conclusion

Introducing a nonuniform rate-dependent frictional property, I can simulate regularly repeating earthquakes at a patch with velocity-weakening friction. These simulated slip events mimic repeating earthquakes in creeping sections along the San Andreas fault, California (e.g., Marone *et al.,* 1995; Nadeau and McEvilly, 1999) and at the Sanriku subduction zone along the Japan trench (Matsuzawa *et al.,* 2002), suggesting that the observed repeating earthquakes occur at velocity-weakening friction patches surrounded by velocity-strengthening friction regions. The simulation shows that the velocity-weakening friction patch is loaded by surrounding aseismic sliding to generate an earthquake, which is followed by significant aseismic sliding in the velocity-strengthening friction region. Aseismic sliding is important for understanding the mechanism of repeating earthquakes.

The duration of simulated slip increases with a decrease in r/r_c, the radius of the velocity-weakening friction patch divided by the critical patch radius for the occurrence of unstable slip. Ordinary, slow, and silent earthquakes with various slip durations can be simulated by the present model. This may explain the wide variety of observed durations of episodic aseismic slip events; several days at the Cascadia subduction zone (Dragert *et al.,* 2001) and beneath the Boso peninsula, central Japan (Sagiya, 1997), 10 months beneath the Bungo channel, southwestern Japan (Hirose *et al.,* 1999), and longer than 18 months beneath the Tokai region, central Japan (Ozawa *et al.,* 2002). From geodetic observations, Miller (2002) reported that silent earthquakes repeatedly occurred with nearly a constant recurrence interval at the Cascadia subduction zone. Many reported silent earthquakes took place in the regions between shallow seismogenic zones and deep aseismic zones (Hirose *et al.,*1999; Dragert *et al.,* 2001; Ozawa, *et al.,* 2002). This may correspond to simulated silent earthquakes in the transitional region of frictional property from velocity-weakening to velocity-strengthening found for Cases 1 and 2 in the present simulation.

Silent earthquakes occur for $r/r_c \sim 0.5$ in the present simulation. Taking r as the source radius of a silent earthquake and putting $r/r_c \sim 0.5$ into Eq (11), I obtain

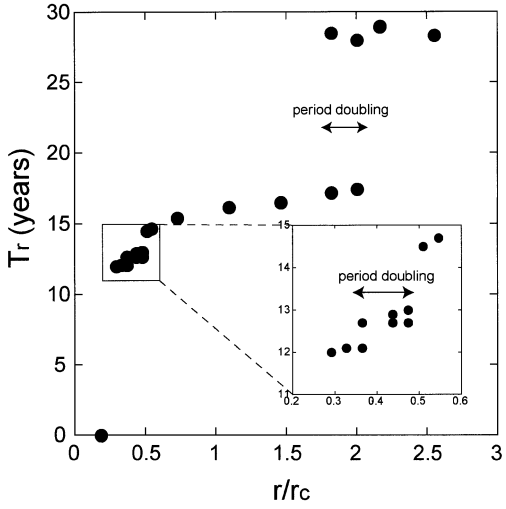

Fig. 17. The recurrence interval T_r of simulated slip events in the circular patch plotted against r/r_c, where r (=5 km) is the radius of a circular patch with a constant negative $A-B$ value and r_c is the critical patch radius defined by Eq. (11).

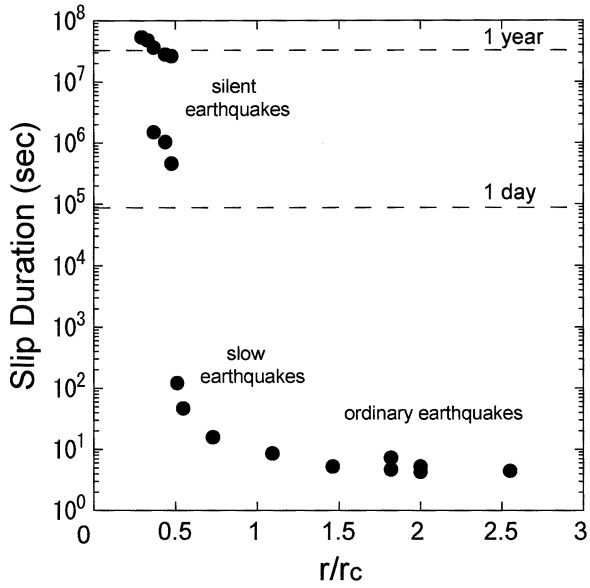

Fig. 18. The duration of simulated slip events versus r/r_c.

$$\frac{D_c}{(B-A)} \sim \frac{48r}{7\pi G}. \tag{13}$$

If an observed silent earthquake takes place at a patch whose size approaches the critical size for unstable slip, Eq. (13) gives a method for estimating frictional constitutive parameters in the Earth. Assuming $G=30$ GPa and $r=30$ km estimated for the silent earthquake beneath the Bongo channel by Hirose *et al.* (1999), I have $D_c/(B-A)=2.2\times10^{-6}$ m/Pa. I further assume $b-a=0.004$, a typical value of granite

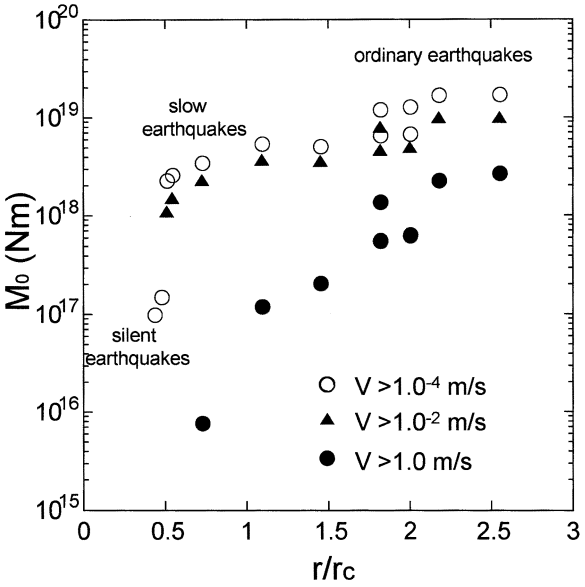

Fig. 19. The seismic moment M_0 of slip events versus r/r_c. M_0 is defined by Eq. (12) with cut-off velocities of 1 m/s, 0.01 m/s, and 10^{-4} m/s.

surface at temperatures below 300℃ (e.g., Blanpied *et al.*, 1995), and $\sigma_n^{eff}=3.5\times10^8$ Pa, which is obtained from lithostatic pressure and hydrostatic pore pressure $\sigma_n^{eff}=(\rho-\rho_w)gz$, where $\rho=2.8\times10^3$ kg/m^3, $\rho_w=1.0\times10^3$ kg/m^3, and $g=9.8$ m/s^2 and $z=20$ km. Finally, I have $D_c=3$ m, which is much larger than those often assumed values of D_c of a few centimeters in seismic cycle simulations (e.g., Tse and Rice, 1986; Stuart, 1988; Kato and Hirasawa, 1997). However, experimental values of $b-a$ depend on rock type and velocity (e.g., Moore *et al.*, 1997) and temperature (e.g., Blanpied *et al.*, 1995), and there is large uncertainty over pore pressure in the Earth (e.g., Rice, 1992). Accordingly, the estimated value of D_c in the present study remains uncertain.

The present model may explain regularly repeating occurrences of ordinary, slow, and silent earthquakes with various slip durations. The observations of postseismic sliding indicate that velocity-weakening friction regions and velocity-strengthening friction regions adjoin at plate boundaries. It is expected that there exist various sizes of velocity-weakening friction regions, where slip events with various slip durations should occur.

Acknowledgements. I am grateful to two anonymous reviewers for useful comments on the manuscript. This research was partly supported by JSPS grant 14340128.

References

Beroza, G.C. and T.H. Jordan, 1990, Searching for slow and silent earthquakes using free oscillations, *J. Geophys. Res.,* **95**, 2485–2510.

Blanpied, M.L., D.A. Lockner and J.D. Byerlee, 1995, Frictional slip of granite at hydrothermal conditions, *J. Geophys. Res.,* **100**, 13045–13064.

Blanpied, M.L., T.E. Tullis and J.D. Weeks, 1998, Effects of slip, slip rate, and shear heating on the friction on granite, *J. Geophys. Res.,* **103**, 489–511.

Byerlee, J.D., 1970, The mechanics of stick-slip, *Tectonophysics,* **9**, 475–486.

Chinnery, M.A., 1969, Theoretical fault models, *Publications of the Dominion Observatory, Ottawa,* **37**, 211–223.

Dieterich, J.H., 1979, Modeling of rock friction 1. Experimental results and constitutive equations, *J. Geophys. Res.,* **84**, 2161–2168.

Dieterich, J.H., 1992, Earthquake nucleation on faults with rate- and state-dependent strength, *Tectonophysics,* **211**, 115–134.

Dragert, H., K. Wang and T.S. James, 2001, A silent slip event on the deeper Cascadia subduction interface, *Science,* **292**, 1525–1528.

Eshelby, J.D., 1957, The determination of the elastic field of an ellipsoidal inclusion, and related problems, *Proc. Roy. Soc., Ser. A,* **241**, 376–396.

Gu, J.-C., J.R. Rice, A.L. Ruina and S.T. Tse, 1984, Slip motion and stability of a single degree of freedom elastic system with rate and state dependent friction, *J. Mech. Phys. Solids,* **32**, 167–196.

Gu, Y. and T.-F. Wong, 1994, Nonlinear dynamics of the transition from stable sliding to cyclic stick-slip in rock, in "*Nonlinera Dynamics and Predictability of Geophysical Phenomena*" *Geophys. Monograph 83, IUGG Vol. 18,* edited by W.I. Newman, A. Gabrielov and D.L. Turcotte, Am. Geophys. Un., Washington, D.C., pp. 15–35.

Heki, K., S. Miyazaki and H. Tsuji, 1997, Silent fault slip following an interplate thrust earthquake at the Japan trench, *Nature,* **386**, 595–598.

Hirose, H., K. Hirahara, F. Kimata, N. Fujii and S. Miyazaki, 1999, A slow thrust slip event following the two 1996 Hyuganada earthquakes beneath the Bungo Channel, southwest Japan, *Geophys. Res. Lett.,* **26**, 3237–3240.

Kato, N. and T. Hirasawa, 1997, A numerical study on seismic coupling along subduction zones using a laboratory-derived friction law, *Phys. Earth Planet. Inter.,* **102**, 51–68.

Kato, N. and T. Hirasawa, 1999, Nonuniform and unsteady sliding of a plate boundary in a great earthquake cycle: A numerical simulation using a rate- and state-dependent friction law, *Pure Appl. Geophys.,* **155**, 93–118.

Kato, N. and T.E. Tullis, 2001, A composite rate- and state-dependent law for rock friction, *Geophys. Res. Lett.,* **28**, 1103–1106.

Kato, N. and T.E. Tullis, 2003, Numerical simulation of seismic cycles with a composite rate- and state-dependent friction law, *Bull. Seismol. Soc. Am.,* **93**, 841–853.

Kawasaki, I., Y. Asai, Y. Tamura, T. Sagiya, N. Mikami, Y. Okada, M. Sakata and M. Kasahara, 1995, The 1992 Sanriku-oki, Japan, ultra-slow earthquake, *J. Phys. Earth,* **43**, 105–116.

Kuroki, H., H.M. Ito and A. Yoshida, 2002, A 3-D simulation of crustal deformation accompanied by subduction in the Tokai region, central Japan, *Phys. Earth Planet. Inter.,* **132**, 39–58.

Lay, T. and H. Kanamori, 1981, An asperity model of large earthquake sequences, in "*Earthquake Prediction: An International Review*" *Maurice Ewing Ser. 4,* edited by D. W. Simpson and P.G. Richards, Am. Geophys. Un., Washington, D. C., pp. 579–592.

Marone, C., 1998, Laboratory-derived friction laws and their application to seismic faulting, *Annu. Rev. Earth Planet. Sci.,* **26**, 643–696.

Marone, C. and B. Kilgore, 1993, Scaling of the critical slip distance for seismic faulting with shear strain in fault zones, *Nature,* **362**, 618–621.

Marone, C., J.E. Vidale and W. Ellsworth, 1995, Fault healing inferred from time dependent variations in source properties of repeating earthquakes, *Geophys. Res. Lett.,* **22**, 3095–3098.

Maruyama, T., 1964, Statical elastic dislocations in an infinite and semi-infinite medium, *Bull. Earthq. Res. Inst.,* **42**, 289–368.

Matsuzawa, T., T. Igarashi and A. Hasegawa, 2002, Characteristic small-earthquake sequence off Sanriku, northeastern Honshu, Japan, *Geophys. Res. Lett.,* **29**, 1543, doi: 10.1029/2001GL014632.

McGarr, A., 1981, Analysis of peak ground motion in terms of a model of inhomogeneous faulting, *J. Geophys. Res.,* **86**, 3901–3912.

Miller, M.M., T. Melbourne, D.J. Johnson and W.Q. Summer, 2002, Periodic slow earthquakes from the Cascadia subduction zone, *Science,* **295**, 2423.

Mitsui, N. and K. Hirahara, 2001,Viscoelastic simulation of earthquake cycle using a simple spring-dashpot-mass system with a friction law, *Geophys. Res. Lett.,* **28**, 4391–4394.

Moore, D.E., D.A. Lockner, S. Ma, R. Summers and J.D. Byerlee, 1997, Strength of serpentine gouges at elevated temperatures, *J. Geophys. Res.,* **102**, 14787–14801.

Neadeau, R.M. and T.V. McEvilly, 1999, Fault slip rates at depth from recurrence intervals of repeating earthquakes, *Science,* **285**, 718–721.

Ozawa, S., M. Murakami, M. Kaidzu, T. Tada, T. Sagiya, Y. Hatanaka, H. Yarai and T. Nishimura, 2002, Detection and monitoring of ongoing aseismic slip in the Tokai region, central Japan, *Science,* **298**, 1009–1012.

Press, W.H., B.P. Flannery, S.A. Teukolsky and W.T. Vetterling, 1992, *Numerical Recipes,* 2nd. ed., Cambridge Univ. Press, New York.

Rice, J.R., 1992, Fault stress state, pore pressure distributions, and the weakness of the San Andreas fault, in "*Fault Mechanics and Transport Properties in Rocks*", edited by B. Evans and T.-f. Wong, Academic Press, San Diego, California, pp. 475–503.

Rice, J.R., 1993, Spatio-temporal complexity of slip on a fault, *J. Geophys. Res.,* **98**, 9885–9907.

Rice, J.R. and A.L. Ruina, 1983, Stability of steady frictional slipping, *J. Appl. Mech.,* **50**, 343–349.

Ruina, A.L., 1983, Slip instability and state variable friction laws, *J. Geophys. Res.,* **88**, 10359–10370.

Sagiya, T., 1997, Boso peninsula silent earthquake of May,

1996, *Eos Trans, AGU,* **78**, Fall Meeting Suppl., F165.
Smetanin, B.I., 1968, Problem of extension of an elastic space containing a plane annular slip, *J. Appl. Math. Mech.,* **32**, 461–466.
Stuart, W.D., 1988, Forecast model for great earthquakes at the Nankai trough subduction zone, *Pure Appl. Geophys.,* **126**, 619–641.
Stuart, W.D. and T.E. Tullis, 1995, Fault model for preseismic deformation at Parkfield, California, *J. Geophys. Res.,* **100**, 24079–24099.
Thatcher, W., 1990, Order and diversity in the models of circum-Pacific earthquake recurrence, *J. Geophys. Res.,* **95**, 2609–2623.
Tse, S.T. and J.R. Rice, 1986, Crustal earthquake instability in relation to the depth variation of frictional slip properties, *J. Geophys. Res.,* **91**, 9452–9472.
Yagi, Y., M. Kikuchi and T. Sagiya, 2001, Co-seismic slip, post-seismic slip, and aftershocks associated with two large earthquakes in 1996 in Hyuga-nada, Japan, *Earth Planets Space,* **53**, 793–803.
Yoshida, S. and N. Kato, 2003, Episodic aseismic slip in a two-degree-of-freedom block-spring model, *Geophys. Res. Lett.,* **30**, 1681, doi: 10.1029/2003GL017439.

(Received February 13, 2003)
(Accepted July 15, 2003)

Appendix A

We obtain shear stress due to uniform slip on a rectangular fault in an infinite elastic medium with Lamé constants λ and μ. Maruyama (1964) showed that the mn component of stress τ_{mn} at the point $Q(x_1, x_2, x_3)$ due to slip $\Delta u_k(P)$ at the point $P(\xi_1, \xi_2, \xi_3)$ on the surface Σ is written by

$$\tau_{mn}(Q)=\int\!\!\int \Delta u_k(P) G_{kl}{}^{mn}(P,Q)\nu_k(P)d\Sigma, \quad \text{(A1)}$$

where ν_k is the kth component of the unit normal vector to the surface $d\Sigma$. Green's function $G_{kl}{}^{mn}(P,Q)$ is

$$G_{kl}{}^{mn}(P,Q)=\frac{\mu}{4\pi}\left[-2(2-3\alpha)\delta_{kl}\delta_{mn}\frac{1}{r^3}+2(1-\alpha)\right.$$
$$(\delta_{km}\delta_{ln}+\delta_{lm}\delta_{kn})\frac{1}{r^3}+6(1-\alpha)(\delta_{kl}r_m r_n+\delta_{mn}r_{kl})\frac{1}{r^5}$$
$$-3(1-2\alpha)(\delta_{km}r_l r_n+\delta_{lm}r_k r_m+\delta_{kn}r_l r_m+\delta_{ln}r_k r_m)$$
$$\left.\frac{1}{r^5}-30\alpha r_k r_l r_m r_n\frac{1}{r^7}\right], \quad \text{(A2)}$$

where $r=[r_1{}^2+r_2{}^2+r_3{}^2]^{1/2}$, $r_k=x_k-\xi_k$, and $\alpha=(\lambda+\mu)/(\lambda+2\mu)$. Let the fault plane be the x_1x_2-plane and the slip direction be x_1, Green's function for 13-component is given by

$$G_{13}{}^{13}(P,Q)=\frac{\mu}{4\pi}\left[2(1-\alpha)\frac{1}{r^3}-3(1-2\alpha)\frac{r_1{}^2+r_3{}^2}{r^5}-\right.$$
$$\left.30\alpha\frac{r_1{}^2 r_3{}^2}{r^7}\right], \quad \text{(A3)}$$

The shear stress τ_{13} at the point Q on the x_1x_2-plane due to uniform slip Δu_1 on a rectangular fault $-L/2\leq\xi_1\leq L/2$, $-W/2\leq\xi_2\leq W/2$, $\xi_3=0$ is

$$\tau_{13}(Q)=\frac{G\Delta u_1}{4\pi}\int_{-L/2}^{L/2}d\xi_1\int_{-W/2}^{W/2}d\xi_2\left[2(1-\alpha)\frac{1}{r^3}-\right.$$
$$3(1-2\alpha)\frac{(x_1-\xi_1)_1{}^2+x_3{}^2}{r^5}-30\alpha$$
$$\left.\frac{(x_1-\xi_1)_1{}^2 x_3{}^2}{r^7}\right]. \quad \text{(A4)}$$

By performing the integration, we obtain

$$\tau_{13}(Q)=\frac{G\Delta u_1}{4\pi}\left\{2(1-\alpha)\left[\frac{\sqrt{(x_1+L/2)^2+(x_2-W/2)^2}}{(x_1+L/2)(x_2-W/2)}-\right.\right.$$
$$\frac{\sqrt{(x_1+L/2)^2+(x_2+W/2)^2}}{(x_1+L/2)(x_2+W/2)}+\frac{\sqrt{(x_1-L/2)^2+(x_2+W/2)^2}}{(x_1-L/2)(x_2+W/2)}$$
$$\left.-\frac{\sqrt{(x_1-L/2)^2+(x_2-W/2)^2}}{(x_1-L/2)(x_2-W/2)}\right]-\frac{1-2\alpha}{(x_1+L/2)}$$
$$\left[\frac{\sqrt{(x_1+L/2)^2+(x_2-W/2)^2}}{x_2-W/2}+\frac{x_2-W/2}{\sqrt{(x_1+L/2)^2+(x_2-W/2)^2}}\right.$$
$$-\frac{\sqrt{(x_1+L/2)^2+(x_2+W/2)^2}}{x_2+W/2}-$$
$$\left.\frac{x_2+W/2}{\sqrt{(x_1+L/2)^2+(x_2+W/2)^2}}\right]-\frac{1-2\alpha}{(x_1-L/2)}$$
$$\left[\frac{\sqrt{(x_1-L/2)^2+(x_2+W/2)^2}}{x_2+W/2}+\frac{x_2+W/2}{\sqrt{(x_1-L/2)^2+(x_2+W/2)^2}}\right.$$
$$-\frac{\sqrt{(x_1-L/2)^2+(x_2-W/2)^2}}{x_2-W/2}-$$
$$\left.\left.\frac{x_2-W/2}{\sqrt{(x_1-L/2)^2+(x_2-W/2)^2}}\right]\right\}. \quad \text{(A5)}$$

Green's function used in Eq. (3) is obtained from (A5).

The stress change at the center of a rectangular fault associated with uniform slip Δu on the fault for $\lambda=\mu$ is obtained from (A5) as follows:

$$\Delta\tau=-\frac{2G\Delta u}{3\pi}\frac{3L^2+4W^2}{LW\sqrt{L^2+W^2}}. \quad \text{(A6)}$$

This coincides with the solution given by Chinnery (1969). Note that Chinnery (1969) took the half length and width of a rectangular fault as parameters instead of the fault length and width.

Appendix B

We obtain the effective stiffness of an annular crack in Appendix B. Smetanin (1968) obtained an approximate solution of the crack opening displacement of an annular crack bounded by two concentric circles, of radii r_1 and r_2 ($r_1 > r_2$), under uniform tensile stress σ:

$$\Delta w(r) = \frac{2(1-\nu^2)}{E} \frac{(r_1 r_2)^{5/4}}{r^{3/2}} \sigma \left(\ln\left(\frac{r_1}{r}\right) \ln\left(\frac{r}{r_2}\right) \right)^{1/2} \Phi\left(\rho \ln\left(\frac{r}{\sqrt{r_1 r_2}} \right) \right), \quad \text{(B1)}$$

where $\rho = 2/\ln(r_1/r_2)$, E is Young's modulus, and $\Phi(t)$ is given by Smetanin (1968). As assumed by McGarr (1981), the dependence of displacement on r_1 and r_2 for an annular shear crack is assumed to be the same as that for an annular tensile crack. From solutions for a penny-shaped crack in extension and shear, $2(1\text{-}\nu^2)/E$ for a tensile crack solution shold be replaced by $12/7G$ for a shear crack solution with $\nu = 0.25$. The relative displacement across an annular shear crack in an infinite elastic medium may be given by

$$\Delta u(r) = \frac{12}{7G} \frac{(r_1 r_2)^{5/4}}{r^{3/2}} \Delta\tau \left(\ln\left(\frac{r_1}{r}\right) \ln\left(\frac{r}{r_2}\right) \right)^{1/2} \Phi\left(\rho \ln\left(\frac{r}{\sqrt{r_1 r_2}} \right) \right). \quad \text{(B2)}$$

To evaluate the effective stiffness ($k_{eff} = \Delta\tau/\Delta u$) of an annular region with transitional values of $A-B$, we put $r_1 = 6$ km, $r_2 = 5$ km, $r = 5.5$ km ($= (r_1 + r_2)/2$) and $G = 30$ GPa into (B2) to obtain $k_{eff} = 35$ MPa/m.